

A Conservative Pressure-Correction Method on Collocated Grid for Low Mach Number Flows

S. M. Yahya¹, S. F. Anwer², S. Sanghi¹

¹Department of Applied Mechanics, Indian Institute of Technology, Delhi, India

²Department of Mechanical Engineering, Zakir Husain College of Engineering & Technology, Aligarh Muslim University, Aligarh, India

Email: yahya_syed@rediffmail.com

Received July 7, 2012; revised August 9, 2012; accepted September 1, 2012

ABSTRACT

A novel extension to SMAC scheme is proposed for variable density flows under low Mach number approximation. The algorithm is based on a predictor—corrector time integration scheme that employs a projection method for the momentum equation. A constant-coefficient Poisson equation is solved for the pressure following both the predictor and corrector steps to satisfy the continuity equation at each time step. The proposed algorithm has second order centrally differenced convective fluxes with upwinding based on Cell Peclet number while diffusive flux are viscous fourth order accurate. Spatial discretization is performed on a collocated grid system that offers computational simplicity and straight forward extension to curvilinear coordinate systems. The algorithm is kinetic energy preserving. Further in this paper robustness and accuracy are demonstrated by performing test on channel flow with non-Boussinesq condition on different temperature ratios.

Keywords: LES; Non-Boussinesq; Low Mach Number; Turbulent Flow

1. Introduction

Various flow regimes in industrial devices are of low speed nature. Such flows are called incompressible, since the velocities are much smaller than the speed of sound. In non-reacting incompressible flows without heat transfer, the use of a pressure-correction algorithm has proven to be accurate and efficient (e.g. [1,2]). Since density remains constant, no substantial problems are encountered and the solution is straightforward. The mass conservation equation naturally imposes a constraint on the velocity field. However, if density varies strongly in time and space, e.g. due to temperature variation, the set of equations becomes more coupled and an efficient solution is no longer obvious. Various attempts have been made to create efficient solution methods. A basic difficulty stems from the acoustic waves in the compressible formulation. As acoustic waves act at a substantially smaller time scale than the convective phenomena in low Mach number flows, the acoustic modes do not significantly influence the solution and may be regarded as superfluous. The use of larger time steps, corresponding to the convective scales, can therefore strongly improve computational efficiency without loss of relevant information.

Furthermore conservation of kinetic energy in numerical methods has become an important issue in large eddy

simulation (LES) and direct numerical simulation (DNS) of turbulence. Kinetic energy conservation in a finite difference formulation is not a consequence of discrete momentum and discrete mass conservation, so conservation of kinetic energy has to be ensured through careful design of the finite difference operators. It is known that dissipative numerical schemes (e.g. up-winding) often introduce too much artificial damping for use in turbulence simulations, because the energy balance in turbulence is rather delicate. In the case of variable density flows, not conserving the kinetic energy can also lead to erroneous temperature and density fields. Much work has been done in the development of kinetic energy conservation algorithms for incompressible flows (see Vasilyev [3]; Gullbrand [4]; Morinishi *et al.* [5]), but there has been less work on variable density or compressible flows (see Nicoud [6] and Lessani [7]). In low-speed turbulent channel flow applications, the low Mach-number, variable-density approximation of the Navier-Stokes equations is a good basis for simulation, as it supports large density variations while eliminating acoustic waves. This eliminates the need for extremely small time steps driven by the acoustics. This means that the arising velocities are much smaller than the speed of sound, so that density variations due to pressure variations can be neglected. In those so-called low Mach number flows, an efficient way

to solve the set of Navier-Stokes equations describing the flow is to use a segregated solver, relying on a pressure-correction algorithm. Here, the pressure is split in a thermodynamic part P_0 and a second order kinematic pressure P_2 , which only appears in the momentum equations. As a result, the momentum equations together with a constraint on the divergence of the velocity decouple from the equations determining the density field. The velocity field is computed from the momentum equations, and is corrected with a pressure-correction to satisfy the divergence constraint. The correction on the pressure is the result of a Poisson-equation, which is elliptic. This paper is organized as follows. Section 2 shows the equations that govern low Mach-number flows, and in Section 3 some details of the numerical method and its implementation are shown. Finally, Section 4 contains test cases and numerical results.

2. Governing Equation

The low Mach-number approximation of the Navier-stokes equations is obtained as the low Mach-number asymptotic limit of the compressible Navier-Stokes equations in which temperature fluctuations are assumed to be of order 1. In this analysis, the pressure is expanded as:

$$P(x, t; M) = P_0(t) + M^2 P_2(x, t) + O(M^3) \quad (2.1)$$

In this expansion, P_0 is the spatially uniform thermodynamic pressure, and P_2 is the hydrodynamic pressure fluctuation. Details of the derivation of these equations can be found in Majda and Sethian [8]; Rehm and Baum [9]; Muller [10] and Paolucci [11]. The final results of this process are the following equations (excluding the body forces):

Conservation of mass:

$$\frac{\partial \rho}{\partial t} + \frac{\partial(\rho u_j)}{\partial x_j} = 0 \quad (2.2)$$

Momentum equation:

$$\frac{\partial \rho u_i}{\partial t} + \frac{\partial(\rho u_i u_j)}{\partial x_j} = -\frac{\partial P_2}{\partial x_i} + \frac{1}{\text{Re}} \frac{\partial \tau_{ij}}{\partial x_j} \quad (2.3)$$

Conservation of energy:

$$\begin{aligned} \rho C_p \frac{\partial T}{\partial t} + \rho C_p u_j \frac{\partial T}{\partial x_j} \\ = \frac{(\gamma - 1)}{\gamma} \left(\frac{dP_0}{dt} \right) + \frac{1}{\text{Re Pr}} \frac{\partial}{\partial x_j} \left(k \frac{\partial T}{\partial x_j} \right) \end{aligned} \quad (2.4)$$

Equation of state:

$$P_0 = \rho T \quad (2.5)$$

In Equations (2.3) and (2.4), Re and Pr are the Reynolds and Prandtl number respectively defined as

$$\text{Re} = \frac{\rho u L}{\mu}, \text{Pr} = \frac{C_p \mu}{k}, \gamma = \frac{C_p}{C_v}$$

τ_{ij} and q_j are the viscous stress tensor and the heat flux vector respectively; and P_2 is the hydrodynamic pressure fluctuation. The low Mach-number both eliminates the acoustic waves and reduces the number of dependent variables by one; this occurs because the energy equation reduces to a constraint, which can be derived by combining Equations (2.2), (2.4) and (2.5) yielding:

$$\frac{\partial u_i}{\partial x_i} = \frac{1}{P_0 C_p} \left[\frac{1}{\text{Re Pr}} \frac{\partial}{\partial x_j} \left(k \frac{\partial T}{\partial x_j} \right) + \left(\frac{\gamma - 1}{\gamma} - C_p \right) \frac{dP_0}{dt} \right] \quad (2.6)$$

For an open system, the thermodynamic pressure (P_0) does not change in time, but in a closed system (sealed enclosure) the thermodynamic pressure can change in time. Notice that the source terms from the energy equation impact the mass conservation equation through the constraint Equation (2.6).

2.1. Large Eddy Simulation (LES) Model

In LES, one computes the motion of large-scale structures, while modeling the non-linear interactions with the small-scales. The governing equations for large eddies are obtained after filtering. The filtering operation can be written in terms of convolution integral:

$$f(x) = \int_D G(x - x') f(x') dx'$$

Large Eddy Simulations have become an important tool for the study of turbulent transport in environmental and engineering flows as it requires coarser mesh than DNS. The basis of such a technique is the application of a spatial filter to the governing equations. An f turbulent variable is splitted into an \tilde{f} large component and f' sub grid component. Note that $\tilde{\cdot}$ corresponds also to the Favre average operator. The non-dimensional forms of the governing Equations (2.2)-(2.5) are then Favre averaged and filtered using implicit filter to obtain governing equations for filtered scale variables.

$$\frac{\partial \bar{\rho}}{\partial t} + \frac{\partial \bar{\rho} \tilde{u}_j}{\partial x_j} = 0 \quad (2.7)$$

$$\begin{aligned} \frac{\partial(\bar{\rho} \tilde{u}_i)}{\partial t} + \frac{\partial(\bar{\rho} \tilde{u}_i \tilde{u}_j)}{\partial x_j} \\ = -\frac{\partial \bar{P}_2}{\partial x_i} + \frac{1}{\text{Re}} \frac{\partial}{\partial x_j} \left[(\mu + \mu_t) \left(2\tilde{S}_{ij} - \frac{2}{3} \tilde{S}_{kk} \delta_{ij} \right) \right] + F \delta_{i1} \end{aligned} \quad (2.8)$$

$$\begin{aligned} & \bar{\rho} C_p \frac{\partial \tilde{T}}{\partial t} + \bar{\rho} C_p \tilde{u}_j \frac{\partial \tilde{T}}{\partial x_j} \\ &= \frac{(\gamma-1)}{\gamma} \left(\frac{\partial P_0}{\partial t} \right) + \frac{1}{\text{Re Pr}} \frac{\partial}{\partial x_j} \left((k+k_t) \frac{\partial \tilde{T}}{\partial x_j} \right) \end{aligned} \quad (2.9)$$

$$P_0 = \bar{\rho} \tilde{T}$$

The flow in the channel is driven by the constant streamwise driving pressure force F . Here the superscript \sim refers to the Favre averaged quantities and \hat{S}_{ij} is the resolved strain rate tensor. Where Favre average is defined as

$$\tilde{f} = \frac{\overline{\rho f}}{\bar{\rho}} \quad (2.10)$$

In the present work, we consider several different sub grid-scale models for thermal part and kinetic part. For modeling sub-grid stresses, we have used Wall Adaptive Layer Equation (WALE) model suggested by Nicoud and Ducros [12]. For thermal part, we have used a dynamic model. In WALE model subgrid scale viscosity accounts for effect of rotation rate and strain rate of the smallest fluctuations. This model has correct wall behavior for sub grid stresses near walls Read [13,14]. WALE model approximates SGS eddy viscosity as

$$\nu_t = \bar{\rho} L_s^2 \frac{(\varsigma_{ij} \varsigma_{ij})^{\frac{3}{2}}}{(S_{ij} S_{ij})^{\frac{5}{2}} + (\varsigma_{ij} \varsigma_{ij})^{\frac{5}{4}}} \quad (2.11)$$

where L_s is a length scale given by

$$L_s = \min \left(kz, C_w V^{\frac{1}{3}} \right) \quad (2.12)$$

where V is the volume of the cell, however $V^{1/3} = \Delta_t$, $k = 0.4187$ is von Karman's constant, z is the distance nearest to the closest wall, $C_w = 0.325$ is the wall constant and ς_{ij} is the traceless symmetric part of the square of the velocity gradient tensor defined as.

$$\varsigma_{ij} = \frac{1}{2} \left(\frac{\partial \tilde{u}_i}{\partial x_k} \frac{\partial \tilde{u}_k}{\partial x_j} + \frac{\partial \tilde{u}_j}{\partial x_k} \frac{\partial \tilde{u}_k}{\partial x_i} \right) - \frac{1}{3} \delta_{ij} \left(\frac{\partial \tilde{u}_l}{\partial x_k} \frac{\partial \tilde{u}_k}{\partial x_l} \right) \quad (2.13)$$

For thermal part we use dynamic Smagorinsky model, the thermal dynamic coupling is taken into account through a similar procedure in order to estimate pr_{SGC} turbulent Prandtl number. The heat flux after the filtering procedure corresponds to

$$E_j = \left(\bar{u}_j \bar{T} - \hat{u} \hat{T}_j \right) \quad (2.14)$$

where pr_{SGS} is given by Equation (2.16) and varies in space and time.

$$P_j = \left[-2\hat{\Delta}^2 \left| \hat{S}_{ij} \right| \frac{\partial \tilde{T}}{\partial x_j} \right] - \left[-2\Delta_t^2 \left| \hat{S}_{ij} \right| \frac{\partial \tilde{T}}{\partial x_j} \right] \quad (2.15)$$

$$pr_{SGS} = -C_{dyn} \frac{\overline{P_j P_j}}{E_j P_j} \quad (2.16)$$

With

$$\lambda_t = \frac{\rho \nu_t C_p}{pr_{SGS}} \quad (2.17)$$

where C_{dyn} is the constant for dynamic Smagorinsky model and λ_t is the sub grid scale diffusivity.

3. Numerical Scheme for Channel Flow

The proposed numerical method is semi-implicit, pressure correction type scheme on a non-staggered structured grid using finite difference scheme for spatial discretisation. The scheme was described by Hirsch [15] and is conceptually similar to the SMAC algorithm described by Amsden and Harlow [16], guided by the work of Cheng and Armfield [17]. It is conceptually similar but an extension to the existing scheme, which is made compatible for low Mach number flows. Here we take full Navier-Stokes equation and then removes acoustic modes from it, as acoustic waves act at a substantially smaller time scale than the convective phenomena in low Mach number flows, the acoustic modes do not significantly influence the solution and may be regarded as superfluous.

3.1. Temporal Descriptisation

The flow field is marched forward in time using a two step predictor—corrector approach. In the predictor step, the time integration of momentum equation is performed using a first order Euler method to obtain the guessed velocity field at the next time step. In the corrector step the guessed velocity fields close to zero. Finally the scheme is given as:

In predictor step guessed momentum flux $(\rho u_{i,j,k})^*$ and guessed velocity vector $u_{i,j,k}^*$ are calculated as

$$\begin{aligned} & (\rho u_{i,j,k})^* \\ &= (\rho u_{i,j,k})^n + \Delta \tau \left\{ H_{i,j,k}^n (\rho^n, u_{i,j,k}^n) - \left(\frac{\partial p}{\partial x_i} \right)^n \right\} \end{aligned} \quad (3.1)$$

where $\Delta \tau = \tau_{n+1} - \tau_n$ and superscripts n , $*$, and $n+1$ denote the known values at the time level n , the predicted or guessed fields and the values at the new time level $n+1$ respectively. The guessed velocity fields do not necessarily satisfy continuity equation. Here, $H_{i,j,k}^n$ is the sum of convective and diffusive fluxes while $f_{i,j,k}^n$ is the

sum of convective and heat transfer fluxes at time level “ n ”. The predicted value for the temperature T^* is calculated from Equation (2.4) based on previous values at time level n ,

$$T_{i,j,k}^* = T_{i,j,k}^n + \frac{\Delta\tau}{\rho^n C_p} \left\{ f_{i,j,k}^n(\rho^n, u_{i,j,k}^n, T^n) + \frac{\gamma}{\gamma-1} \left(\frac{P_0^n - P_0^{n-1}}{\Delta\tau} \right) \right\} \quad (3.2)$$

Guessed thermodynamic pressure and guessed density field would be

$$P_0^* = \frac{M_0}{\int \frac{dV}{T^*}} \quad \rho^* = \frac{P_0^*}{T^*}$$

In this step guessed velocity field obtained in the predictor step is corrected in a continuity preserving manner, firstly we define correction flux and correction pressure

$$F' = (\rho u)' = (\rho u)_{i,j,k}^{n+1} - (\rho^* u^*)_{i,j,k} = F_{i,j,k}^{n+1} - F_{i,j,k}^* \quad (3.3)$$

And

$$P' = P_{i,j,k}^{n+1} - P_{i,j,k}^n \quad (3.4)$$

The velocity and temperature field at time level $n + 1$ that satisfies continuity is coupled to the pressure field at anew time level $n + 1$ through a semi explicit discretisation in time of the momentum equations. This is given by,

$$T_{i,j,k}^{n+1} = T_{i,j,k}^n + \frac{\Delta\tau}{\rho^n C_p} \left\{ f_{i,j,k}^n(\rho^n, u_{i,j,k}^n, T^n) + \frac{\gamma}{\gamma-1} \left(\frac{P_0^n - P_0^{n-1}}{\Delta\tau} \right) \right\} \quad (3.5)$$

$$(\rho u_{i,j,k})^{n+1} = (\rho u_{i,j,k})^n + \Delta\tau \left\{ H_{i,j,k}^n(\rho^n, u_{i,j,k}^n) - \left(\frac{\partial p}{\partial x_i} \right)^{n+1} \right\} \quad (3.6)$$

The relationship between velocity and pressure correction (P') can be obtained by subtracting Equation (3.1) from (3.6). This yields

$$F_{i,j,k}^{n+1} - F_{i,j,k}^* = -\Delta\tau \frac{\partial P'}{\partial x_i}$$

$$F' = -\Delta\tau \frac{\partial P'}{\partial x_i} \quad (3.7)$$

Taking divergence of the above Equation (3.7) with the discrete divergence operator defined as below

$$\Delta_d = \frac{\partial}{\partial x_i}$$

$$\Delta_d \cdot (F_{i,j,k}^{n+1} - F_{i,j,k}^*) = -\Delta\tau \left(\Delta_d \cdot \frac{\partial P'}{\partial x_i} \right)$$

$$\nabla^2 P' = -\frac{1}{\Delta\tau} \Delta_d F'$$

Now using continuity equation and defined correction flux we get

$$\nabla^2 P' = -\frac{1}{\Delta\tau} \left(\left(\frac{\partial \rho^*}{\partial \tau} \right) - \left(\frac{\partial \rho}{\partial \tau} \right)^{n+1} \right) \quad (3.8)$$

where below mentioned value of density is used in Poisson equation

$$P_0^{n+1} = \frac{M_0}{\int \frac{dV}{T^{n+1}}} \quad \rho^{n+1} = \frac{P_0^{n+1}}{T^{n+1}}$$

For a closed system, like ours, the thermodynamic pressure p_0 is calculated by using

$$P_0^n = \frac{M_0}{\int \frac{dV}{T^n}} \quad P_0^{n-1} = \frac{M_0}{\int \frac{dV}{T^{n-1}}}$$

$$\frac{dP_0}{dt} = \frac{P_0^n - P_0^{n-1}}{\Delta\tau} \quad (3.9)$$

3.2. Spatial Descritisation

The spatial discretization is performed using finite difference methodology on a collocated mesh with a Cartesian coordinate system. The up-winding scheme employs two points in upstream and one point on the downstream side of the grid under-consideration. Convective fluxes are second order centrally differenced; the choice between up-winding and central differencing is made on the basis of cell Peclet number while diffusive fluxes are viscous fourth order accurate. The discrete Poisson equation is differenced as

$$\frac{\delta}{\delta x_i} \left(\frac{\partial P'}{\partial x} \right) = \frac{1}{\delta x_1} \left\{ \left(\frac{\partial P'}{\partial x} \right)_{i+\frac{1}{2},j,k} - \left(\frac{\partial P'}{\partial x} \right)_{i-\frac{1}{2},j,k} \right\} \quad (3.10)$$

where

$$\left(\frac{\partial P'}{\partial x} \right)_{i+\frac{1}{2},j,k} = \frac{P'_{i+1,j,k} - P'_{i,j,k}}{\delta x_2} \quad (3.11)$$

$$\left(\frac{\partial P'}{\partial x} \right)_{i-\frac{1}{2},j,k} = \frac{P'_{i,j,k} - P'_{i-1,j,k}}{\delta x_3}$$

$$\delta x_1 = \frac{x_{i+1} - x_{i-1}}{2}, \quad \delta x_2 = \frac{x_{i+1} - x_i}{2}, \quad \delta x_3 = \frac{x_i - x_{i-1}}{2}$$

Convective flux are second order centrally differenced given below

$$f_{i,j,k}^n = \frac{(\rho u)_R^n u_{i+1}^n - (\rho u)_L^n u_i^n}{\Delta x} + k \frac{T_{i+1}^n - 2T_i^n + T_{i-1}^n}{\Delta x^2} \quad (3.12)$$

where the subscripts R and L indicate extrapolated values at the right and left face of the control volume. For first order upwinding, and positive values of the velocity, this means

$$(\rho u)_R = \rho_{i+\frac{1}{2}} u_{i+\frac{1}{2}} \quad \text{and} \quad (\rho u)_L = \rho_{i-\frac{1}{2}} u_{i-\frac{1}{2}}$$

with averaged face density values:

$$\rho_{i+\frac{1}{2}} = (\rho_i + \rho_{i+1})/2$$

The node velocities are calculated by averaging:

$$u_i = \left(u_{i-\frac{1}{2}} + u_{i+\frac{1}{2}} \right) / 2$$

Diffusive fluxes are viscous fourth order accurate which is calculated as follows:

$$H_{i,j,k} = \frac{1}{\text{Re}} \frac{\tau_{i+1,j,k} - \tau_{i,j,k}}{\Delta x}$$

$$\tau_{i,j,k} = \mu \frac{-u_{i+2,j,k} + 8u_{i+1,j,k} - 8u_{i-1,j,k} + u_{i-2,j,k}}{12\Delta x} + O(\Delta x^4) \quad (3.13)$$

4. Results and Discussion

Three numerical experiments were performed in order to test the numerical scheme and its implementation. We used self made FORTRAN code for TLES (thermal large eddy simulation). A mesh of size $96 \times 96 \times 96$ is used for simulation purpose, uniform meshes are used in the stream-wise and span-wise directions and a non-uniform mesh with hyperbolic tangent distribution is used in the wall-normal direction. For the velocities, no slip boundary condition was used on the top and bottom walls and periodic boundary condition was used in x - y direction. The temperatures on the hot and cold walls were set according to R_θ . Viscosity was calculated using Sutherlands law with reference at T_c . The reference Reynolds number based on the reference velocity and channel half width is kept constant at 2800 while the Prandtl number is fixed at 0.71.

First, a 1D convection-diffusion problem was set to test spatial and temporal convergence in a variable density case. Second, a 2D inviscid solenoidal velocity field was used to test kinetic energy conservation. Finally, a 3D turbulent channel flow with large temperature gradient is used.

4.1. Spatial and Temporal Convergence in 1D

The test problem for this experiment is a temperature profile that will be convected in the x -direction. For simplicity the flow was assumed to be inviscid and the domain was the interval $[0, 1]$. The initial temperature pro-

file is a Gaussian given by equation.

$$T(k) = 295 + 50 \exp \left[- \left(\frac{x-0.5}{0.05} \right)^2 \right] \quad (4.1)$$

The velocity in the x -direction (u) was set equal to 1; the hydrodynamic pressure was set to 0 Pa and the thermodynamic pressure was set to 1. The working fluid was assumed to be air so that its thermal conductivity (k) could be estimated from polynomial correlations. Since the thermal diffusivity of air is $O(1 \times 10E-05)$, the global Peclet number is very high $O(1 \times 10E-05)$. For the spatial convergence the grid was changed from 100, 200, 400 to 800 nodes while the time step was held in 0.00125 so that the CFL number changed from 0.125 to 1. For the temporal convergence the mesh was held in 100 grid points and the time was changed from 0.005 to 0.000625 so that the CFL number changed from 0.5 to 0.0625. **Figure 1** shows the profile of velocity at $t = 1$ for four different time steps. The velocity induced by the diffusion process was of the order 1×10^{-6} . The shape of the u -velocity profile is in agreement with the theory and what is expected from Equation (4.1). **Table 1** summarizes the numerical results from this experiment.

4.2. Kinetic Energy Conservation

For this numerical experiment a 2-dimensional rectangular domain $[0, 1] \times [0, 1]$ is used, with an initial steady state solenoidal velocity field given by Equation (4.2).

$$u(x, y) = -\cos(2\pi x) \sin(2\pi y)$$

$$v(x, y) = \sin(2\pi x) \cos(2\pi y) \quad (4.2)$$

The temperature field was set as a Gaussian random field with a mean value of 397 K and a root mean square fluctuation of 57 K. The density field can be computed from the equation of state. Using Equation (4.2) and the initial random density field, the initial kinetic energy can be computed ($KE_0 = 0.2274$ J). A mesh of 24×24 points was used, so that $\Delta x = \Delta y = 4.2e-02$. According to Nicoud [6], the integration time for this numerical experiment is given by Equation (4.3).

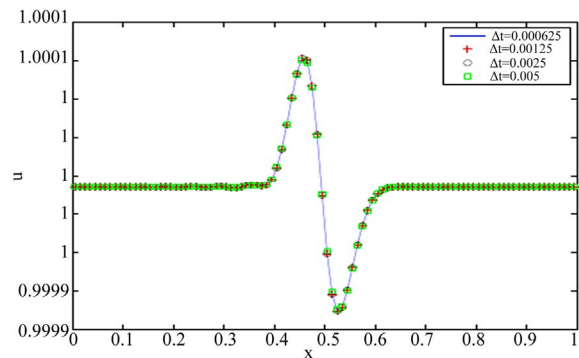


Figure 1. “ u ” velocity profile.

$$t = \frac{0.125L}{\sqrt{KE_0}} = 0.3125s \quad (4.3)$$

Table 2 and **Figure 2** show the results for this experiment. It is evident that the scheme conserves global kinetic energy, so that the divergence-free constraint is recovered in the inviscid limit.

The error in **Table 2** was calculated using the ratio between the difference in the initial and final kinetic energy *i.e.*

$$\text{ERROR} = \frac{KE_0 - KE_f}{KE_0}$$

4.3. 3D Channel Flow Simulation

In this section, we present detailed numerical results from the test problems that we considered in order to check the robustness and accuracy of the proposed algorithm. This is the case of large-eddy simulation (LES) of non-isothermal, turbulent channel flow with strong temperature gradients due to the temperature difference between the two walls.

In this subsection, we consider turbulent flow in a channel whose walls are kept at different temperatures. This problem is treated numerically with the help of LES. Let x , y and z , denote the stream-wise, span-wise and normal directions, respectively. The dimensions of the domain are $4\pi\delta \times 4/3\pi\delta \times 2\delta$, with δ being the half width of the channel. The walls of the channel are normal to the z direction and are held at constant temperature. The boundaries of the domain normal to the x and y directions are periodic in nature. Therefore, the total mass of the system is conserved, *i.e.*, this is an example of flow in a closed domain. A mesh of 64^3 points is used in such a way that $\Delta x^+ \times \Delta y^+ \times \Delta z^+ = 33 \times 11 \times [05:11]$. Uniform meshes are used in the stream-wise and span-wise directions and a non-uniform mesh with hyperbolic

Table 1. Spatial and temporal convergence rates.

	u	v	T
Spatial	1.971	1.954	1.881
Temporal	0.967	0.942	0.977

Table 2. Numerical results from KE conservation.

Δt	CFL	KE_0	KE_f	ERROR
0.04166	1	0.2274	0.226879	2.59×10^{-03}
0.02083	0.5	0.2274	0.226891	2.54×10^{-03}
0.004166	0.1	0.2274	0.226918	2.42×10^{-03}
0.002083	0.05	0.2274	0.226921	2.40×10^{-03}
0.0004166	0.01	0.2274	0.226927	2.38×10^{-03}

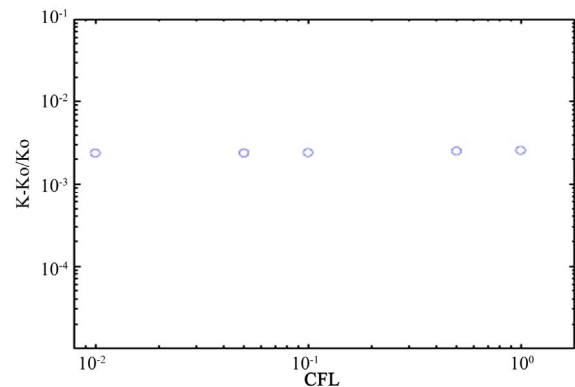


Figure 2. Error of the KE as a function of CFL.

tangent distribution is used in the wall-normal direction. The Wall-Adapting Local Eddy-viscosity (W-ALE) model (Nicoud [12]) is used for modeling the eddy viscosity and dynamic Smagorinsky method is used to model turbulent heat flux. In the homogeneous directions, the convective terms of the momentum and energy equations are calculated using hybrid type upwind. The multi-grid algorithm (Jameson [18]) is used to solve the constant-coefficient pressure Poisson equation. Let T_h and T_c denote the temperatures of the hot and cold walls, respectively. Two different cases, corresponding to different wall temperature ratios, are considered herein. Specifically, $R_\theta = 1.01$ and $R_\theta = 2$. Here, $R_\theta = T_h/T_c$. For all the simulations $T_m = (T_h + T_c)/2$ is used to initialize the flow field. **Table 1** represents important simulation parameters. For comparison purposes between our results and with the Direct Numerical Simulations (DNS) data, we used a molecular Prandtl number of 0.7 for the first case ($T_h/T_c = 1.01$) and Sutherland law for the case ($T_h/T_c = 2$). The $R_\theta = 1.01$ results are compared with the DNS of Kim *et al.* [19] and Lessani [20], while $R_\theta = 2$ results are compared with DNS of Nicoud [21] as shown in **Table 3**.

Figure 3 shows that $R_\theta = 1.01$ is in good agreement with previous incompressible DNS (Kim *et al.*, [19]) for the mean velocity profile. The expected (for the friction Reynolds number considered) law-of-the-wall $u^+ = 2.5 \ln(y^+) + 5.5$ is recovered. The viscous sub layer is also well resolved as shown in **Figure 3**. **Figure 4** shows a good agreement with previous incompressible DNS (Kim *et al.*, [19]) for the three velocity fluctuations and the Reynolds shear stress. For any instantaneous variable ϕ , $\langle \phi \rangle$ denotes the time and space averaged field. Space averaging is performed in the homogenous direction and fluctuating field is defined as $\phi' = \phi - \langle \phi \rangle$, hence $\phi_{rms} = \langle \phi' \phi' \rangle^{1/2}$. The mean stream-wise velocity is

$$u^+ = \frac{\langle u \rangle}{u_\tau}$$

Table 3. Simulation parameters and physical parameters.

Reference	Temperature ratio (R_θ)	Mesh	Mesh in wall units	Bulk Reynolds number (Re_b)	Centerline Reynolds number (Re_c)	$\frac{U_{zH} - U_\tau}{\bar{U}_\tau}$	$Re_\tau H - Re_\tau C$
Present	1.01	64^3	$33 \times 11 \times [05:11]$	2800	3200	0.99 - 1.0	179 - 181
Present	2	64^3	$33 \times 11 \times [05:11]$	2121	2559	0.87 - 1.13	92 - 234
Kim <i>et al.</i> (1987)	Isothermal	$192 \times 160 \times 128$	$12 \times 7 \times [0.05:4.4]$	2800	3200	0.86 - 1.16	178.12
Nicoud (1998)	1.01	$120 \times 100 \times 120$	$18.8 \times 6.28 \times [0.25 - 10]$	2800	3300	0.89 - 1.12	180 - 180
Nicoud (1998)	2	$120 \times 100 \times 120$	$18.8 \times [2.8 - 7.2] \times [0.25 - 10]$	2800	2700	0.87 - 1.13	82 - 200

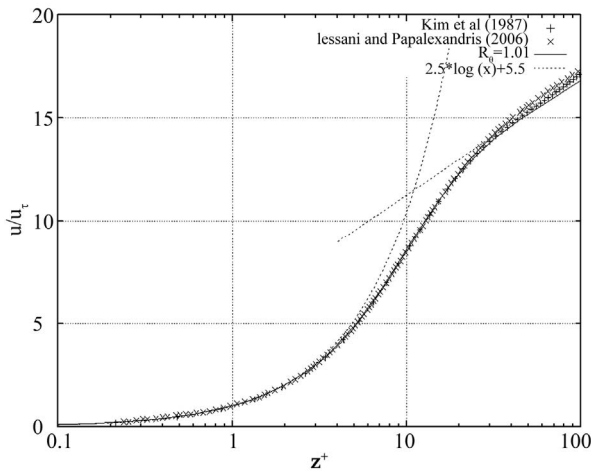


Figure 3. Mean velocity profile in log units for $R = 1.01$ with $u^+ = z^+$ and $u^+ = 2.5 \ln z^+ + 5.5$.

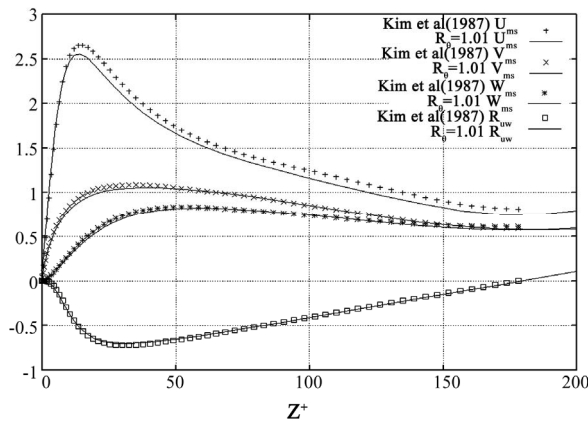


Figure 4. Variation of turbulent stresses ($\langle u'^2 \rangle, \langle v'^2 \rangle, \langle w'^2 \rangle, \langle u'w' \rangle$) along normal direction (z^+) for $R_\theta = 1.01$.

while turbulent intensities are defined as

$$\frac{u_{rms}}{u_\tau}, \frac{v_{rms}}{u_\tau}, \frac{w_{rms}}{u_\tau}$$

and temperature fluctuations are defined as

$$\frac{T_{rms}}{T_\tau}$$

Figures 5-9 show variations of different quantities in the channel for $R_\theta = 2$. Figure 5 shows mean velocity profile and Figure 6 shows temperature profile for the entire channel. Both are in good agreement with previous DNS of Nicoud [21]. Figure 7 shows Mean velocity profile (u^+) with the classical scaling. For the cold side of the channel, law-of-the-wall $u^+ = 2.5 \ln(z^+) + 5.5$ is recovered but with a different constant while in the hot side of the logarithmic nature of law-of-the-wall is small. This agrees with the previous DNS. The viscous sub layer is also well resolved as shown in Figure 7. Figure 9 shows good agreement of RMS velocities along the wall normal direction. It can be seen that agreement with the published literature is much better in the cold channel than the hot channel. There is a good qualitative agreement between present work and DNS. The discrepancy is always less than 5%. Figure 8 shows temperature fluctuations along the wall normal direction. There is a qualitative agreement while the peak fluctuating intensities don't match. There is deviation in the core of the channel and the hotter channel side. These deviations can be due to different bulk and channel centerline velocities obtained. Further as the comparison is from the DNS which is far more accurate than LES.

5. Conclusion

In this article, a new algorithm which extends the exist

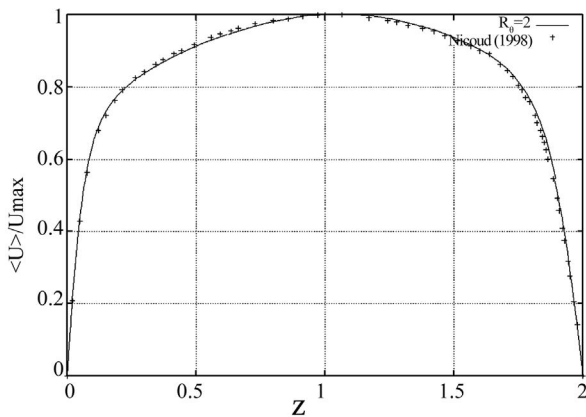


Figure 5. Mean Stream-wise velocity profile normalized with maximum velocity for the entire channel.

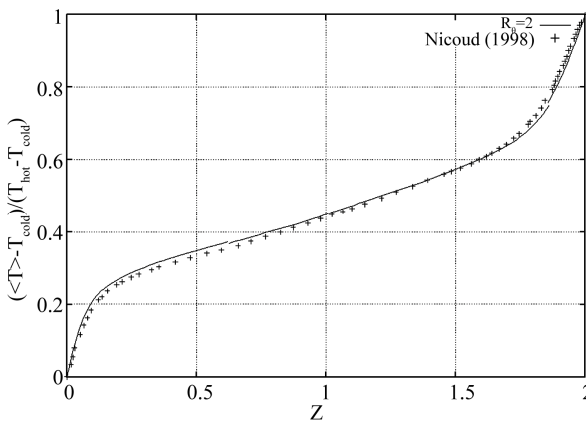


Figure 6. Mean Temperature for $\frac{\langle T \rangle - T_c}{\Delta T}$ for the entire channel along wall normal direction, for $R_\theta = 2$.

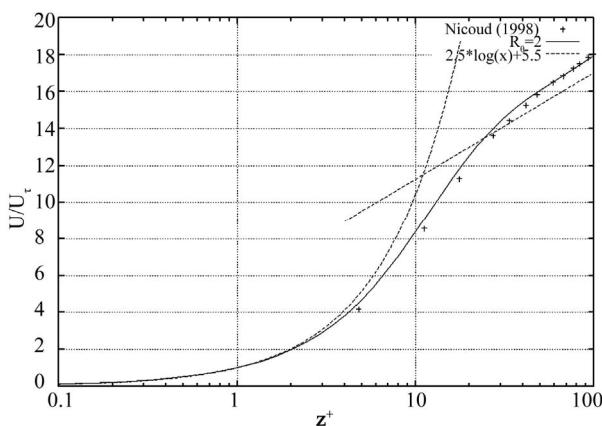


Figure 7. Mean velocity profile in log units along the channel for $R_\theta = 2$.

ing SMAC scheme for low Mach number, variable density flows has been presented. This algorithm can be applied to both open and closed domains. It is based on a two-stage predictor—corrector method. This algorithm is

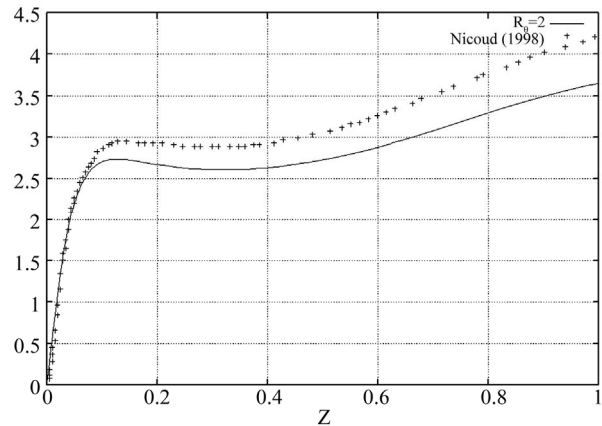


Figure 8. Variation of T_{rms} along the wall normal direction (z^+) for $R_\theta = 2$.

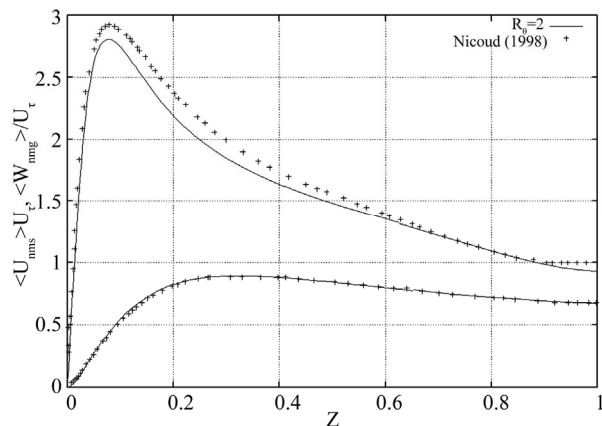


Figure 9. Variation of RMS velocities along the wall normal direction (z) for $R_\theta = 2$.

particularly useful for unsteady flows with strong temperature gradients. A constant-coefficient Poisson equation, which is computationally more efficient than the variable-coefficient one, is solved for the pressure. A collocated grid is used for spatial discretization and not a staggered one because collocated grids offer computational simplicity and straightforward extension to curvilinear coordinate systems. The odd-even decoupling problem is avoided by using smartly a continuity equation in conjunction with correction flux. The robustness and accuracy of the algorithm have been assessed through simulations of three test problems; 1D convection-diffusion problem, 2D steady state solenoidal velocity distribution for conservation of kinetic energy and finally the turbulent channel flow with temperature gradients. The results obtained with the proposed algorithm are in very good agreement with the ones reported in earlier studies. The algorithm has a moderate computational cost for solving the Poisson-equation and is stable for high density ratios (at least up to a factor of 10). Though in the examples shown in this paper, P_0 was always a constant

this algorithm can be extended to problems in which P_0 depends on time, by integrating the equation of state.

REFERENCES

- [1] A. J. Chorin, "On the Convergence of Discrete Approximations to the Navier-Stokes Equations," *Mathematics of Computations*, Vol. 23, No. 106, 1969, pp. 342-353. [doi:10.1090/S0025-5718-1969-0242393-5](https://doi.org/10.1090/S0025-5718-1969-0242393-5)
- [2] A. J. Chorin, "Numerical Solution of the Navier-Stokes Equations," *Mathematics of Computations*, Vol. 22, No. 104, 1968, pp. 745-762. [doi:10.1090/S0025-5718-1968-0242392-2](https://doi.org/10.1090/S0025-5718-1968-0242392-2)
- [3] O. V. Vasilyev, "High Order Finite Difference Schemes on Non-Uniform Meshes with Good Conservative Properties," *Journal of Computational Physics*, Vol. 157, No. 2, 2000, pp. 746-761. [doi:10.1006/jcph.1999.6398](https://doi.org/10.1006/jcph.1999.6398)
- [4] J. Gullbrand, "An Evaluation of a Conservative Fourth Order DNS Code in Turbulent Channel Flow," *Center for Turbulence Research Annual Research Briefs*, NASA Ames/Stanford University, 2000, pp. 211-218.
- [5] Y. Morinishi, T. S. Lund, O. V. Vasilyev and P. Moin, "Fully Conservative Higher Order Finite Difference Schemes for Incompressible Flow," *Journal of Computational Physics*, Vol. 143, No. 1, 1998, pp. 90-124. [doi:10.1006/jcph.1998.5962](https://doi.org/10.1006/jcph.1998.5962)
- [6] F. Nicoud, "Conservative High-Order Finite-Difference Schemes for Low-Mach Number Flows," *Journal of Computational Physics*, Vol. 158, No. 1, 2000, pp. 71-97. [doi:10.1006/jcph.1999.6408](https://doi.org/10.1006/jcph.1999.6408)
- [7] B. Lessani, J. Ramboer and C. Lacor, "Efficient Large-Eddy Simulations of Low Mach Number Flows Using Preconditioning and Multigrid," *International Journal of Computational Fluid Dynamics*, Vol. 18, No. 3, 2004, pp. 221-223. [doi:10.1080/10618560310001654319](https://doi.org/10.1080/10618560310001654319)
- [8] A. Majda and J. Sethian, "The Derivation and Numerical Solution of the Equations for Zero Mach Number Combustion," *Combustion Science and Technology*, Vol. 42, No. 3-4, 1985, pp. 185-205. [doi:10.1080/00102208508960376](https://doi.org/10.1080/00102208508960376)
- [9] R. G. Rehm and H. R. Baum, "The Equation of Motion for Thermally Driven Buoyant Flows," *Journal of Research of the National Bureau of Standards*, Vol. 83, No. 3, 1978, pp. 297-308.
- [10] B. Müller, "Low-Mach Number Asymptotics of the Navier-Stokes Equations," *Journal of Engineering Mathematics*, Vol. 34, No. 1-2, 1998, pp. 97-109. [doi:10.1023/A:1004349817404](https://doi.org/10.1023/A:1004349817404)
- [11] S. Paolucci, "Filtering of Sound from the Navier-Stokes Equations," Sandia National Laboratories, Livermore, 1982.
- [12] F. Nicoud and F. Ducros, "Subgrid-Scale Stress Modeling Based on the Square of Velocity Gradient Tensor," *Flow Turbulence and Combustion*, Vol. 62, No. 3, 1999, pp. 183-200. [doi:10.1023/A:1009995426001](https://doi.org/10.1023/A:1009995426001)
- [13] M. Germano, U. Piomelli, P. Moin and W. H. Cabot, "A Dynamic Subgrid-Scale Eddy Viscosity Model," *Physics of Fluids A*, Vol. 3, No. 7, 1991, pp. 1760-1765. [doi:10.1063/1.857955](https://doi.org/10.1063/1.857955)
- [14] P. Moin, K. Squires, W. Cabot and S. Lee, "A Dynamic Subgrid-Scale Model for Compressible Turbulence and Scalar Transport," *Physics of Fluids*, Vol. 3, No. 11, 1991, pp. 2746-2757. [doi:10.1063/1.858164](https://doi.org/10.1063/1.858164)
- [15] C. Hirsch, "Numerical Computation of Internal and External Flows," John Wiley & Sons Inc., Hoboken, 1990.
- [16] A. A. Amsden and F. H. Harlow, "The SMAC Method: A Numerical Technique for Calculating Incompressible Fluid Flows," Los Alamos Scientific Laboratory of the University of California, Los Alamos, 1970.
- [17] L. Cheng and S. Armfield, "A Simplified Marker and Cell Method for Unsteady Flows on Non-Staggered Grids," *International Journal for Numerical Methods in Fluids*, Vol. 21, No. 1, 1995, pp. 15-34. [doi:10.1002/flid.1650210103](https://doi.org/10.1002/flid.1650210103)
- [18] A. Jameson, "Time Dependent Calculations Using Multigrid, with Applications to Unsteady Flows past Airfoils and Wings," *Proceedings of 10th Computational Fluid Dynamics Conference*, Honolulu, 24-26 June 1991, pp. 91-1596.
- [19] J. Kim, P. Moin and R. Moser, "Turbulence Statistics in Fully Developed Channel Flow at Low Reynolds Number," *Journal of Fluid Mechanics*, Vol. 177, 1987, pp. 133-166. [doi:10.1017/S0022112087000892](https://doi.org/10.1017/S0022112087000892)
- [20] B. Lessani and M. V. Papalexandris, "Time-Accurate Calculation of Variable Density Flows with Strong Temperature Gradients and Combustion," *Journal of Computational Physics*, Vol. 212, No. 1, 2006, pp. 218-246. [doi:10.1016/j.jcp.2005.07.001](https://doi.org/10.1016/j.jcp.2005.07.001)
- [21] F. C. Nicoud, "Numerical Study of a Channel Flow with Variable Properties," Center for Turbulence Research Annual Research Briefs, 1998, pp. 289-310.